Spline finite strip method incorporating different plate theories for thick piezoelectric composite plates

G. Akhras* and W. C. Li

Department of Civil Engineering, Royal Military College of Canada
P.O. Box 17000, STN Forces, Kingston, Ontario, K7K 7B4, Canada

Abstract.   In the present analysis, the spline finite strip with higher-order shear deformation is formulated for the static analysis of piezoelectric composite plates. The proposed method incorporates Reddy's third-order shear deformation theory, Touratier's "Sine" model, Afaq's exponential model, Cho's higher-order zigzag laminate theory, as well as the classic plate theory and the first-order plate theory. Thus, the analysis can be conducted based on any of the above-mentioned theories. The selection of a specific method is done by simply changing a few terms in a 2 by 2 square matrix and the results, obtained according to different plate theories, can be compared to each other. Numerical examples are presented for piezoelectric composite plates subjected to mechanical loading. The results based on different shear deformation theories are compared with the three-dimensional solutions. The behaviours of piezoelectric composite plates with different length-to-thickness ratios, fibre orientations, and boundary conditions are also investigated in these examples.

Keywords: piezoelectric composite plate; spline finite strip method; Reddy's third-order shear deformation theory; Touratier's plate theory; Afaq's plate theory; Cho's higher-order zigzag laminate theory.

1. Introduction

In recent years, the promising application of piezoelectric effects in structural monitoring and control systems has drawn increased attention from many engineers and researchers to develop accurate and more efficient analysis methods for investigating the behaviours of piezoelectric composite plates (Kogl and Bucalem 2005).

For the analysis of thick composite plates, the classical thin plate theory and the first-order shear deformation theory often yield unacceptable results, because the former totally neglects the transverse shear deformation while the latter only assumes a constant transverse shear strain in the thickness direction of plate.

In 1984, Reddy introduced the third-order shear deformation theory (Reddy 1984), which assumes a parabolic variation of the transverse shear strains through the plate thickness, and takes into account the vanished transverse shear stresses on the plate surfaces. Based on Reddy's theory, analytical solutions have been obtained for simply supported cross-ply laminates and anti-symmetrical angle-ply laminates. The results are satisfactory in comparison with the three-dimensional elasticity solutions for thick laminates with the length-to-thickness ratio as low as 4, while the number of degrees of freedom

*Corresponding author, E-mail: Akhras@rmc.ca

required in the analysis is the same as the one using the first-order plate theory. In addition, the shear correction coefficients adopted by the first-order plate theory also become unnecessary. As the plate becomes relatively thinner, the solution converges to the result according to the thin plate theory automatically. In later years, Touratier proposed a "Sine" model (1991), whereas Afaq, et al. (2003) introduced an exponential model, by respectively assuming sinusoidal and exponential variations of inplane displacement in the thickness direction, yielding further improved accuracy. In 1993, Cho developed a higher-order zigzag laminate theory by superimposing a zigzag linearly varying in-plane displacement on a cubic varying displacement field (Cho and Parmerter 1993). The cubic variation accounts for the overall parabolic distribution of transverse shear strains, while the zigzag simulates the strain discontinuities required by stress continuity conditions. The unknowns of different planes are expressed in terms of those of midplane after imposing the interlaminar shear stress continuity conditions and ensuring the plate surfaces free of transverse shear stresses. In this way, the number of required degrees of freedom remains unchanged, but a continuous distribution of shear stresses is achieved. Consequently, the accuracy of analysis is further improved with only limited additional calculations. However, all the above-mentioned higher-order theories experience difficulties in their finite element implementation, because the required shape functions must guarantee the inter-element continuity not only for the deflection but also for its first derivatives. Formulation of such finite elements often requires extra degrees of freedom and lengthy calculation (Phan and Reddy 1985, Sheikh and Chakrabarti 2003), causing additional computational efforts.

The problems can be easily solved by modeling the plate structure with a number of longitudinal spline finite strips (Cheung, et al. 1996). Within each strip, a series of B-spline functions are used to express the displacement variations in the longitudinal direction, while the Hermitian cubic polynomials are employed to interpolate the deflection variation in the lateral in-plane direction. Thus, the deflection and its first derivatives are all continuous across the nodal lines between the finite strips. The spline finite strip method has been successfully employed to incorporate Reddy's third-order shear deformation for the analysis of thick isotropic and laminated plates by Kong and Cheung in 1993. The approach was then applied to the analysis of piezolaminated plates by Ramos Loja, et al. (2001). However, in all these works, only the results on simply supported cross-ply laminates were presented in the application of this method to thick composite plates. Ramos Loja, et al. (2001, 2002) also published the spline strips using Lo's higher order shear deformation theory for thick angle-ply laminates. Since eleven degrees of freedom are used for each node in order to define the structural deformation of the strip, the efficiency of the analysis could be further improved.

Recently, a new spline finite strip with higher-order shear deformation has been developed by the authors for the analysis of composite plates using Reddy's third-order shear deformation theory and Cho's zigzag theory (Akhras and Li 2005, 2007). The strip has three nodal lines, each of which has an identical number of knots (Fig. 1). The knot on a side nodal line has six degrees of freedom, while the knot on the middle nodal line has four degrees of freedom only. This means that the present method employs approximately the same number of degrees of freedom as the spline finite strip method based on the first-order shear deformation theory (Dawe 2002), but will yield improved results for thick composite plates. In the lateral in-plane direction, the quadratic interpolation is adopted for the in-plane displacements, while the Hermitian interpolation is employed for the deflection. This interpolation combination can accurately simulate a linear variation of the transverse bending moment in the lateral in-plane direction for all types of laminates, so that the convergence of the analysis is enhanced.

In the current study, this spline finite strip method is extended to the analysis of piezoelectric composite plates. The electric potentials on the surfaces and middle plane of each piezoelectric layer
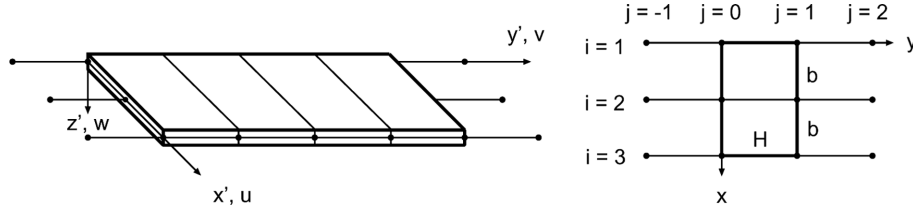
Fig. 1 A spline finite strip (on the left) and a section (on the right)

are added as nodal degrees of freedom. If a continuous electrode is installed on the surface of the layer, the electric potential on the surface is taken as a global degree of freedom, so as to automatically satisfy the equipotential condition on the electrode. The proposed method incorporates Reddy's third-order shear deformation theory, Touratier's "Sine" model, Afaq's exponential model, Cho's higher-order zigzag laminate theory, as well as the first-order plate theory and the classical thin plate theory. Thus, the analysis can be conducted based on any of the above-mentioned plate theories selected by simply switching the items in a 2 by 2 square matrix, and the results can be compared with those according to other plate theories.

The numerical examples are presented for piezoelectric composite plates subjected to mechanical loading. The results based on different shear deformation theories are compared with three-dimensional solutions. Effects of length-to-thickness ratios, fibre orientations, and boundary conditions on the behaviour of piezoelectric composite plates are also investigated in these examples.

2. Spline finite strip method incorporating different plate theories

In the spline finite strip analysis, the plate structure is modeled by a number of longitudinal strips. The proposed spline finite strip has three equally spaced nodal lines, labelled by $i = 1, 2, 3$ respectively (Fig. 1). In the longitudinal direction, the strip is divided into a number of sections of identical length H. Within a section, the displacement components at any point are interpolated from the displacement parameters at 12 knots located on the three nodal lines at local coordinates $y = j H$ with j equal to -1, 0, 1 and 2, respectively. In addition to these nodal displacement parameters, the electric potentials on the surfaces and middle plane of each piezoelectric layer are also taken as nodal degrees of freedom. However, if a continuous electrode is installed on the surface of the piezoelectric layer, the electric potential within the electrode is uniform (Fig. 2). Because the electrode may cover many sections or even entire area of the layer, it is convenient to take the electric potential in the electrode as a global degree of freedom, so that the equipotential condition on the electrode is automatically satisfied, and the total number of required degrees of freedom can be reduced significantly. Thus, for the knot identified by i and j, the following generalized displacement parameters are adopted:

$$\{\delta\}_{ij} = \begin{cases} \left[u_o, v_o, w_o, \dfrac{\partial w_o}{\partial x}, \gamma_x, \gamma_y, \dots \phi_{1k}, \phi_{2k}, \phi_{3k} \dots \right]^T_{ij} & \text{for } i = 1, 3 \\[2mm] \left[u_o, v_o, \gamma_x, \gamma_y, \dots \phi_{1k}, \phi_{2k}, \phi_{3k} \right]^T_{ij} & \text{for } i = 2 \end{cases} \tag{1}$$

where u_o, v_o, w_o denote the midplane displacement components in the directions as shown in Fig. 1, γ_x and γ_y represent the transverse shear deformation measured at midplane of the plate, whereas ϕ_{1k}, ϕ_{2k}
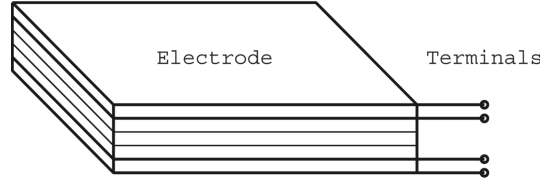
Fig. 2 Electrodes in piezoelectric laminate

and ϕ_{3k} ($k = 1$ to n) are respectively the electric potentials on the top surface, the midplane and the bottom surface of the kth piezoelectric layer at the knot, and n is the total number of piezoelectric layers in the plate. If any continuous electrode is installed, the corresponding electric potential should be removed from the above expression and represented by a global degree of freedom.

Within a section, the midplane displacements u_o, v_o, w_o, the midplane shear deformation γ_x, γ_y, and the electric potential ϕ_k in the kth piezoelectric layer can be expressed in terms of the generalized displacement parameters as

$$u_o = \sum_{i=1}^{3} \sum_{j=-1}^{2} N_i(x)\Phi_j(y)u_{ij}$$

$$v_o = \sum_{i=1}^{3} \sum_{j=-1}^{2} N_i(x)\Phi_j(y)v_{ij}$$

$$w_o = \sum_{i=1,3} \sum_{j=-1}^{2} \left[W_i(x)\Phi_j(y)w_{ij} + R_i(x)\Phi_j(y)\left(\frac{\partial w}{\partial x}\right)_{ij} \right]$$

$$\gamma_x = \sum_{i=1}^{3} \sum_{j=-1}^{2} N_i(x)\Phi_j(y)\gamma_{xij}$$

$$\gamma_y = \sum_{i=1}^{3} \sum_{j=-1}^{2} N_i(x)\Phi_j(y)\gamma_{yij}$$

$$\phi_k = \sum_{i=1}^{3} \sum_{j=-1}^{2} \sum_{m=1}^{3} N_i(x)\Phi_j(y)L_{mk}(z)\phi_{mkij} \qquad (2)$$

where $N_i(x)$ for $i = 1, 2, 3$ are the quadratic interpolation functions defined as:

$$N_1(x) = (b-x)(2b-x)/(2b^2)$$
$$N_2(x) = x(2b-x)/b^2$$
$$N_3(x) = x(x-b)/(2b^2) \qquad (3)$$

and b is the spacing between two adjacent nodal lines (see Fig. 1);
$W_i(x)$ and $R_i(x)$ for $i = 1, 3$ are the following Hermitian cubic polynomials:

$$W_1(x) = 1 - 3(\bar{x})^2 + 2(\bar{x})^3$$

$$W_3(x) = 3(\bar{x})^2 - 2(\bar{x})^3$$

$$R_1(x) = x[1 - 2(\bar{x}) + (\bar{x})^2]$$

$$R_3(x) = x[(\bar{x})^2 - (\bar{x})] \tag{4}$$

and $\bar{x} = x/2b$;

$\Phi_j(y)$ for j = -1, 0, 1, 2 denote B-spline functions, which have the following expressions within the section with $y \in [0, H]$:

$$\Phi_{-1}(y) = \frac{1}{6H^3}(H-y)^3$$

$$\Phi_0(y) = \frac{1}{6H^3}[H^3 + 3H^2(H-y) + 3H(H-y)^2 - 3(H-y)^3]$$

$$\Phi_1(y) = \frac{1}{6H^3}[H^3 + 3H^2y + 3Hy^2 - 3y^3]$$

$$\Phi_2(y) = \frac{1}{6H^3}y^3 \tag{5}$$

The required spline functions for unequal lengths of section are provided in (Cheung, *et al.* 1996); $L_{1k}(z)$, $L_{2k}(z)$ and $L_{3k}(z)$ are the quadratic interpolation functions in the z direction defined as:

$$L_{1k}(z) = (z-z_{2k})(z-z_{3k})/(z_{1k}-z_{2k})(z_{1k}-z_{3k})$$

$$L_{2k}(z) = (z-z_{1k})(z-z_{3k})/(z_{2k}-z_{1k})(z_{2k}-z_{3k})$$

$$L_{3k}(z) = (z-z_{1k})(z-z_{2k})/(z_{3k}-z_{1k})(z_{3k}-z_{2k}) \tag{6}$$

in which z_{1k}, z_{2k} and z_{3k} are respectively the z-coordinates of the top surface, the midplane and the bottom surface of the kth piezoelectric layer.

Displacements u, v and w at any point (x, y, z) in the laminate have the following relationships with the midplane displacements:

$$\{u\} = \{u_o\} - z\{w'\} + [F(z)]\{\gamma\}$$

$$w = w_0(x, y) \tag{7}$$

where $\{u\} = [u, v]^T$, $\{w'\} = \left[\frac{\partial w}{\partial x}, \frac{\partial w}{\partial y}\right]^T$, $\{\gamma\} = [\gamma_x, \gamma_y]^T$, while $[F(z)]$ is a 2 by 2 matrix describing the variation of transverse deformation through the plate thickness.

Reddy's theory (Reddy 1984) assumes a parabolic variation of transverse shear strains through plate thickness. Therefore, $[F(z)]$ has the following form:

$$F(z)_{11} = F(z)_{22} = z\left(1 - \frac{4z^2}{3h^2}\right) \quad \text{and} \quad F(z)_{12} = F(z)_{21} = 0 \tag{8}$$

in which h is the plate thickness.

Touratier's model (Touratier 1991) assumes a cosine variation of transverse shear strains. Thus, $[F(z)]$ is

written as:

$$F(z)_{11} = F(z)_{22} = \frac{h}{\pi}\sin\left(\frac{\pi z}{h}\right) \text{ and } F(z)_{12} = F(z)_{21} = 0 \tag{9}$$

Afaq's model (Afaq, *et al.* 2003) introduces an exponential variation of inplane displacement in the thickness direction, and $[F(z)]$ has the following form:

$$F(z)_{11} = F(z)_{22} = ze^{-2(z/h)^2} \text{ and } F(z)_{12} = F(z)_{21} = 0 \tag{10}$$

Cho's theory (Cho and Parmerter 1993) superimposes a zigzag linearly varying in-plane displacement on a cubic varying displacement field, yielding continuous distribution of transverse shear stresses in the thickness direction of plate. $[F(z)]$ takes a more complicated form as follows (Shu and Sun 1994):

$$[F(z)]_k = [F_1]_k + z[F_2]_k + z^2[F_3] + z^3[F_4] \tag{11}$$

in which, the subscript k represents the ordinal number of a layer, while $[F_1]_k$, $[F_2]_k$, $[F_3]$ and $[F_4]$ are determined from the material properties and laminate thicknesses as below:

$$[F_3] = 4[h[C_1]_N + 4[C_2]_N]^{-1}[C_2]_N/h,$$

$$[F_4] = -4[h[C_1]_N + 4[C_2]_N]^{-1}[C_1]_N/3h,$$

$$[F_2]_k = 2([Q_{sk}]^{-1}[C_1]_k - z_k[I])[F_3] + 3(2[Q_{sk}]^{-1}[C_2]_k - z_k^2[I])[F_4],$$

$$[F_1]_k = \sum_{l=2}^{k} z_{l-1}([F_2]_{l-1} - [F_2]_l) - \sum_{l=2}^{m} z_{l-1}([F_2]_{l-1} - [F_2]_l)$$

and

$$[C_1]_k = \sum_{l=1}^{k} [Q_{sl}](z_l - z_{l-1})$$

$$[C_2]_k = \sum_{l=1}^{k} [Q_{sl}](z_l^2 - z_{l-1}^2)/2 \tag{12}$$

where, N is the number of layers in the laminate, z_k is the z coordinate of the interface between layer k and layer $k+1$, $[I]$ is the unit matrix, m is the ordinal number of the layer across or next to the plate midplane ($z_m = 0$ or $z_m z_{m+1} < 0$), $[Q_{sk}]$ is the transverse shear stiffness matrix of layer k defined by $[\tau_{xz},\ \tau_{yz}]^T = [Q_{sk}][\gamma_{xz},\ \gamma_{yz}]^T$.

Eq. (7) is also applicable to the analysis based on the classical plate theory by assuming

$$F(z)_{11} = F(z)_{12} = F(z)_{21} = F(z)_{22} = 0 \tag{13}$$

as well as for the analysis using the first-order shear deformation theory by taking

$$F(z)_{11} = F(z)_{22} = z \text{ and } F(z)_{12} = F(z)_{21} = 0 \tag{14}$$

Thus, the analysis can be conducted based on any above-mentioned theory selected by simply switching

the contents of matrix $[F(z)]$, and the results obtained according to different plate theories can be compared to each other.

Within the laminate, the generalized displacements have the following linear relationships with the generalized strains:

$$\varepsilon_x = \frac{\partial u}{\partial x}, \; \varepsilon_y = \frac{\partial v}{\partial y}, \; \gamma_{xy} = \frac{\partial u}{\partial y} + \frac{\partial v}{\partial x}, \; \gamma_{yz} = \frac{\partial v}{\partial z} + \frac{\partial w}{\partial y}, \; \gamma_{zx} = \frac{\partial u}{\partial z} + \frac{\partial w}{\partial x}$$

$$-E_x = \frac{\partial \phi}{\partial x}, \; -E_y = \frac{\partial \phi}{\partial y}, \; -E_z = \frac{\partial \phi}{\partial z} \tag{15}$$

where E_x, E_y and E_z are the components of electric field. By taking into consideration Eqs. (2), (7) and the above relationships, the generalized strain vector at any point within a section can be expressed in terms of the nodal and global degrees of freedom in the following matrix form:

$$\{\bar{\varepsilon}\} = [\varepsilon_x, \varepsilon_y, \gamma_{xy}, \gamma_{yz}, \gamma_{zx}, -E_x, -E_y, -E_z]^T = [\bar{B}]_s \{\bar{\delta}\}_s \tag{16}$$

in which $[\bar{B}]_s$ is the generalized sectional strain matrix, while $\{\bar{\delta}\}_s$ is the vector of generalized sectional displacement parameters, including the nodal degrees of freedoms at 12 knots and the electric potentials on the continuous electrodes across the section.

Derivation shows that, at any given coordinate z, ε_x varies linearly in the x direction, so that the current formulation can accurately simulate a linear variation of the transverse bending moment in the lateral in-plane direction. Consequently, the convergence of the analysis can be improved significantly over the strips using linear interpolations in the x direction for the in-plane displacements (Kong and Cheung 1993, Ramos Loja, *et al*. 2001). This is especially important for the analysis of composite laminates with coupling between bending and in-plane deformation.

It is assumed that the plate is composed of orthotropic layers (or plies). Neglecting σ_z, for each layer, the generalized stress-strain relationships in the x-y-z coordinate system can be stated as

$$\{\bar{\sigma}\} = \begin{Bmatrix} \sigma_x \\ \sigma_y \\ \tau_{xy} \\ \tau_{yz} \\ \tau_{zx} \\ D_x \\ D_y \\ D_z \end{Bmatrix} = \begin{bmatrix} \bar{Q}_{11} & \bar{Q}_{12} & \bar{Q}_{16} & 0 & 0 & 0 & 0 & \bar{e}_{31} \\ \bar{Q}_{12} & \bar{Q}_{22} & \bar{Q}_{26} & 0 & 0 & 0 & 0 & \bar{e}_{32} \\ \bar{Q}_{16} & \bar{Q}_{26} & \bar{Q}_{66} & 0 & 0 & 0 & 0 & \bar{e}_{36} \\ 0 & 0 & 0 & \bar{Q}_{44} & \bar{Q}_{45} & \bar{e}_{14} & \bar{e}_{24} & 0 \\ 0 & 0 & 0 & \bar{Q}_{45} & \bar{Q}_{55} & \bar{e}_{15} & \bar{e}_{25} & 0 \\ 0 & 0 & 0 & \bar{e}_{14} & \bar{e}_{15} & -\eta_{xx} & -\eta_{xy} & 0 \\ 0 & 0 & 0 & \bar{e}_{24} & \bar{e}_{25} & -\eta_{xy} & -\eta_{yy} & 0 \\ \bar{e}_{31} & \bar{e}_{32} & \bar{e}_{36} & 0 & 0 & 0 & 0 & -\eta_{zz} \end{bmatrix} \begin{Bmatrix} \varepsilon_x \\ \varepsilon_y \\ \gamma_{xy} \\ \gamma_{yz} \\ \gamma_{zx} \\ -E_x \\ -E_y \\ -E_z \end{Bmatrix} = [\bar{Q}]\{\bar{\varepsilon}\} \tag{17}$$

where D_x, D_y and D_z are the components of electric displacement, while η_{xx}, η_{xy}, η_{yy} and η_{zz} are the components of electric permittivity. The coefficients in the $\bar{Q}$ matrix can be calculated from the elastic moduli, Poisson's ratios, piezoelectric moduli, dielectric constants of the lamina and ply orientations (Kogl and Bucalem 2005, Kant and Swaminathan 2001, Reddy 2004). The required equations are given in the Appendix, for the reader's convenience.

Then, the generalized stiffness matrix of the section can be formed as (Kogl and Bucalem 2005):

$$[K]_s = \iiint_V [\bar{B}]_s^T [\bar{Q}][\bar{B}]_s dV \tag{18}$$

whereas the sectional load vector $\{P\}_s$ due to external loads can be formed in the same way as the elastic analysis (Ramos Loja, *et al.* 2001, 2002).

After assembling the stiffness matrices and load vectors over all the sections in the structure, followed by imposing boundary conditions (Cheung, *et al.* 1996), the generalized nodal displacement parameters and electrode potentials can be determined by solving the structural equilibrium matrix equation in the form as:

$$[K]\{\delta\} = \{P\} \tag{19}$$

Thereafter, the generalized displacements, strains and stresses at any point within the plate structure can be computed by means of Eqs. (2), (7), (15) and (17).

3. Numerical examples

3.1. Example 1: Simply supported square (0º/90º/90º/0º) laminate under sinusoidal load

The example with exact 3D solution of Pagano (1970) is selected here to verify the convergence of the proposed method. A square (0º/90º/90º/0º) laminate of thickness h and side length $a = 4.0h$ is simply supported on four edges and subjected to a sinusoidal vertical pressure $p_z = P\sin\frac{\pi x}{a}\sin\frac{\pi y}{a}(N/m^2)$ on the top surface with the origin of the coordinate system being located at the lower left corner on the midplane. All the layers have identical thickness. The material properties are assumed to be $E_1 = 25.0E_2$, $G_{12} = G_{13} = 0.5E_2$, $G_{23} = 0.2E_2$, $v_{12} = v_{13} = 0.25$.

By virtue of symmetry, only a quarter of the laminate is analyzed. In each case, one to four proposed spline strips are employed with the number of sections equal to the number of strips. The resulting dimensionless maximum deflections and stresses are listed in Table 1 using the following abbreviations:

$$\bar{w} = 10^2 wh^3 E_2/Pa^4 \text{ at } (a/2, a/2, 0), \quad \bar{\sigma}_4 = \tau_{yz}h/Pa \text{ at } (a/2,0,0)$$

$$\bar{\sigma}_1 = \sigma_x h^2/Pa^2 \text{ at } (a/2, h/2, h/2), \quad \bar{\sigma}_5 = \tau_{zx}h/Pa \text{ at } (0,a/2,0)$$

$$\bar{\sigma}_2 = \sigma_y h^2/Pa^2 \text{ at } (a/2, a/2, h/4), \quad \bar{\sigma}_6 = \tau_{xy}h^2/Pa^2 \text{ at } (0,0,h/2)$$

The three-dimensional solution of Pagano (3D) and a converged finite element solution of Topdar, *et al.* (2004) based on a refined higher-order shear deformation theory (RHSDT 2004) are also given in the table for comparison.

It can be seen that the present finite strip solutions based on all the shear deformation theories converge rapidly to the respective analytical solutions (Analytical), some of which are obtained by the authors using the variational method based on the principle of virtual displacements (Reddy 2004) and incorporating exact in-plane interpolations as assumed displacement functions. It is obvious that all the higher-order shear deformation theories yield improved accuracy over the first-order shear deformation theory (FSDT with shear correction coefficients $k_1^2 = k_2^2 = 5/6$) and the classic plate theory (CLPT).

Table 1 Deflection & stresses in simply supported (0º/90º/90º/0º) square laminate (a/h=4) under sinusoidal load

Theory	Method	$\bar{w}$	$\bar{\sigma}_1$	$\bar{\sigma}_2$	$\bar{\sigma}_4$	$\bar{\sigma}_5$	$\bar{\sigma}_6$
Reddy's TSDT	1×1 Section	1.9105	0.7669	0.6638	0.2499	0.2123	0.0473
	2×2 Sections	1.8957	0.6969	0.6369	0.2391	0.2068	0.0448
	3×3 Sections	1.8941	0.6800	0.6338	0.2390	0.2064	0.0444
	4×4 Sections	1.8945	0.6738	0.6395	0.2393	0.2065	0.0439
	Analytical (Reddy 1984, 2004)	1.8937	0.6651	0.6322	0.2389	0.2064	0.0440
Touratier's Sine Model	1×1 Section	1.9260	0.7861	0.6416	0.2670	0.2225	0.0448
	2×2 Sections	1.9146	0.7168	0.6568	0.2535	0.2172	0.0447
	3×3 Sections	1.9108	0.6987	0.6485	0.2479	0.2166	0.0448
	4×4 Sections	1.9096	0.6919	0.6424	0.2466	0.2164	0.0449
	Analytical	1.9088	0.6830	0.6349	0.2462	0.2163	0.0450
Afaq's Exponential Model	1×1 Section	1.9369	0.8066	0.6443	0.2745	0.2327	0.0457
	2×2 Sections	1.9251	0.7351	0.6592	0.2603	0.2274	0.0457
	3×3 Sections	1.9213	0.7165	0.6506	0.2550	0.2267	0.0457
	4×4 Sections	1.9201	0.7095	0.6444	0.2535	0.2266	0.0458
	Analytical	1.9193	0.7004	0.6367	0.2533	0.2264	0.0459
Cho's Zigzag Theory	1×1 Section	1.9236	0.8506	0.7186	0.2494	0.2351	0.0425
	2×2 Sections	1.9117	0.7736	0.7275	0.2360	0.2307	0.0430
	3×3 Sections	1.9080	0.7538	0.7164	0.2302	0.2300	0.0431
	4×4 Sections	1.9069	0.7464	0.7091	0.2288	0.2299	0.0432
	Analytical (Shu and Sun 1994)	1.9060	0.7368	0.7001	0.2284	0.2298	0.0434
Elasticity	Analytical (Pagano 1970)	1.954	0.720	0.663	0.292	0.219	0.0467
RHSDT	FEM (Topdar, *et al*. 2004)	1.9059	-	-	-	-	-
FSDT	Analytical	1.7100	0.4059	0.5765	0.1963	0.1394	0.0308
CLPT	Analytical	0.4312	0.539	0.269	-	-	0.0213

3.2. Example 2: Simply supported square (p/0º/90º/p) laminate under sinusoidal load

   The example partly analyzed by Heyliger (1994) is presented here to further assess the performance of the proposed method. A square piezoelectric laminate of thickness $h = 1$ m and side length a is simply supported on four edges (SSSS), and subjected to a sinusoidal vertical pressure $p_z = P \sin\frac{\pi x}{a} \sin\frac{\pi y}{a} (N/m^2)$ on the top surface. The value of h is selected by Heyliger arbitrarily for simplicity in calculation and presentation. The laminate consists of a [0º/90º] Graphite-Epoxy sublaminate and two PZT-4 outer layers. Each elastic layer has a thickness of 0.4 h, whereas each piezoelectric layer has thickness of 0.1h. The material properties are given in Table 2. The outer surface of each piezoelectric layer is grounded with the electric potential there being forced to equal zero, whereas the inner surface is unelectroded with freely varying potential. In addition, the vertical edges of the plate are also grounded with the electric potential equal to zero.

   By virtue of symmetry, only a quarter of the laminate is analyzed. In each case, one to three proposed spline strips are employed with the number of sections equal to the number of strips. The dimensionless maximum deflections $100w_{max}h^3E_{2,Gr-Ep}/(Pa^4)$ for different length-to-thickness ratios a/h are determined based on aforementioned shear deformation theories. The results are presented in Table 3. The exact three-dimensional solution of Heyliger (3D) and the converged three-dimensional finite layer solutions

Table 2 Elastic and piezoelectric properties of materials in Example 2 to Example 5.

	Elastic Properties			Piezoelectric Properties	
Properties	Graphite-Epoxy	PZT-4	Properties	Graphite-Epoxy	PZT-4
E_1 (GPa)	132.38	81.3	e_{31} (C/m^2)	0	-5.20
E_2 (GPa)	10.756	81.3	e_{32} (C/m^2)	0	-5.20
E_3 (GPa)	10.756	64.5	e_{33} (C/m^2)	0	15.08
G_{12} (GPa)	5.654	30.6	e_{15} (C/m^2)	0	12.72
G_{23} (GPa)	3.606	25.6	e_{24} (C/m^2)	0	12.72
G_{31} (GPa)	5.654	25.6	η_{11}/η_o	3.5	1475
v_{12}	0.24	0.329	η_{22}/η_o	3.0	1475
v_{13}	0.24	0.432	η_{33}/η_o	3.0	1300
v_{23}	0.49	0.432			

Table 3 Simply supported square (p/0°/90°/p) laminate under unit sinusoidal load

a/h	Mesh	$100w_{max}h^3E_{2,Gr-Ep}/(Pa^4)$			
		Reddy's TSDT	Touratier's Sine Model	Afaq's Model	Cho's Zigzag Theory
	1×1 Section	1.2375	1.2385	1.2347	1.3127
	2×2 Sections	1.2225	1.2228	1.2184	1.2936
	3×3 Sections	1.2171	1.2179	1.2138	1.2900
4	Analytical	1.2106	1.2115	1.2075	1.2864
	3D (Heyliger 1994)		1.2616		
	FSDT		0.9535		
	CLPT		0.5019		
	1×1 Section	0.6382	0.6386	0.6383	0.6511
	2×2 Sections	0.6231	0.6234	0.6229	0.6351
	3×3 Sections	0.6201	0.6205	0.6201	0.6325
10	Analytical	0.6163	0.6167	0.6163	0.6292
	3D FLM (Akhras and Li 2007)		0.6262		
	FSDT		0.5740		
	CLPT		0.5017		
	1×1 Section	0.5230	0.5230	0.5230	0.5232
	2×2 Sections	0.5086	0.5086	0.5086	0.5087
	3×3 Sections	0.5057	0.5057	0.5057	0.5059
100	Analytical	0.5028	0.5028	0.5028	0.5029
	3D FLM (Akhras and Li 2007)		0.5029		
	FSDT		0.5024		
	CLPT		0.5016		

(3D FLM (2007)) are also given in the table for comparison.

It can be seen that the convergence of the present finite strip solutions is generally good. It is apparent that the higher-order shear deformation theories result in a better accuracy than FSDT and CLPT. In addition, it can be noted that Cho's zigzag theory leads to the most accurate results for the thick cross-ply piezoelectric laminates.

Table 4 Dimensionless deflection $\bar{w} = 100 w_{\max} h^3 E_{2,Gr-Ep}/(Pa^4)$ and electric potential ϕ (mV) at the top center of simply supported square ($p/0^o/90^o/0^o/p$) laminate under unit sinusoidal load

Electric conditions	a/h=4		a/h=10		a/h=100	
	$\bar{w}$	ϕ	$\bar{w}$	ϕ	$\bar{w}$	ϕ
Closed-circuit	1.3460	0.000	0.6392	0.000	0.4996	0.000
Open-circuit, unelectroded	1.2853	0.067	0.5794	0.778	0.4422	76.30
Open-circuit, continuous electrode	1.3082	0.029	0.6060	0.169	0.4679	16.49
Elastic solutions	1.3479	-	0.6397	-	0.4999	-

3.3. Example 3: Simply supported square (p/0º/90º/0º/p) laminate under sinusoidal load: Effects of the electric conditions

A simply supported (SSSS) square ($p/0^o/90^o/0^o/p$) piezoelectric laminate of thickness $h = 0.01$ m and side length a is selected to investigate the effects of the electric conditions. The laminate consists of a [$0^o/90^o/0^o$] Graphite-Epoxy sublaminate and two PZT-4 outer layers. Each elastic layer has a thickness of $0.2667\,h$, whereas each piezoelectric layer has thickness of $0.1h$. The material properties, boundary conditions and load are identical to those in the previous example. In all the considered cases, the inner surface of each piezoelectric layer is always grounded. However, the outer surface of the layer may be grounded (closed-circuit condition) or remains free (open-circuit condition). In addition, the outer surface may be unelectroded or covered with a continuous electrode. In the former case, the electric potential varies on the surface, while in the latter case, the electric potential remains constant on the entire surface. The analysis is conducted based on Cho's zigzag laminate theory with a quarter of laminate being modeled by 4×4 sections. The resulting dimensionless deflection $\bar{w} = 100 w_{\max} h^3 E_{2,Gr-Ep}/(Pa^4)$ and electric potential ϕ (in mV) at the center of the top surface due to $P = 1 N/m^2$ are listed in Table 4. The elastic solutions with piezoelectric effects being totally neglected are also given in this table for comparison.

Results show that the piezoelectricity has little stiffening effects for the laminate with closed circuits, while it reduces $w_{\max}$ of the unelectroded laminate under open-circuit condition by 11.5% for the thin plate, and 4.6% for the thick plate. The piezoelectricity also reduces $w_{\max}$ of the laminate with open-circuited continuous electrodes by 6.4% for the thin plate, and 2.9% for the thick plate. This means that the piezoelectricity has more significant stiffening effects for the unelectroded laminate than that with continuous electrodes.

It can also be observed that the piezoelectricity induces much higher maximum electric potential in the unelectroded laminate than that with continuous electrodes. The ratio of the maximum electric voltages in the former to the latter is as high as 4.63.

3.4. Example 4: Clamped square (p/0º/90º/p) laminate under sinusoidal load

The square five-layer ($p/0^o/90^o/0^o/p$) laminate in the previous example is clamped on its four edges (CCCC) with load and all other conditions remaining unchanged. Both the closed-circuit condition and open-circuit condition are considered. A quarter of the laminate is modelled by four proposed strips with four longitudinal sections each. In addition, for the clamped edges, all the degrees of freedom are fixed, and $w'_y = 0$ is also imposed on the clamped edge normal to the y axis.

The dimensionless deflection $\bar{w} = 100 w_{\max} h^3 E_{2,Gr-Ep}/(Pa^4)$ and the electric potential ϕ (in mV) at the center of the top surface due to $P = 1\, N/m^2$ are determined based on Cho's zigzag theory and presented

Table 5 Dimensionless deflection $\overline{w} = 100w_{max}h^3E_{2,Gr-Ep}/(Pa^4)$ and electric potential ϕ (mV) at the top center of clamped square ($p/0°/90°/0°/p$) laminate under unit sinusoidal load

Electric conditions	a/h=4		a/h=10		a/h=100	
	$\overline{w}$	ϕ	$\overline{w}$	ϕ	$\overline{w}$	ϕ
Closed-circuit	0.9340	0.000	0.3012	0.000	0.1600	0.000
Open-circuit, unelectroded	0.9034	0.014	0.2881	0.337	0.1483	23.35
Open-circuit, continuous electrodes	0.9320	0.005	0.3013	0.011	0.1600	0.655
Elastic solutions	0.9370	0.000	0.3016	0.000	0.1601	0.000

in Table 5. The elastic solutions are also given in the table for comparison.

Results reveal that the piezoelectricity has little stiffening effect for the clamped laminate with continuous electrodes, and the induced electrode potential is relatively low. This may be attributed to the fact that the piezoelectric effects on the surface areas with tensile stress and compressive stress have cancelled out each other. Therefore, the continuous electrode is inefficient in the clamped laminates.

3.5. Example 5: Six layer square piezoelectric laminates with different fibre-orientations subjected to sinusoidal load

Simply supported (SSSS) square piezoelectric laminates of thickness $h = 0.01$ m and side length a are all subjected to a sinusoidal vertical pressure $p_z=P\sin\frac{\pi x}{a}\sin\frac{\pi y}{a}(N/m^2)$ on the top surface. Each laminate consists of a four layer Graphite-Epoxy sublaminate and two PZT-4 outer layers. Each elastic layer has a thickness of 0.2 h, whereas each piezoelectric layer has thickness of 0.1h. The material properties are given in Table 2. Four types of laminate with the fibre-orientations ($p/0°/90°/90°/0°/p$), ($p/0°/90°/0°/90°/p$), ($p/45°/-45°/45°/-45°/p$) and ($p/45°/-45°/-45°/45°/p$) respectively are considered. The entire laminate is analyzed using eight proposed strips with eight sections each based on Reddy's third order shear deformation theory. On each edge, the plate is free to rotate about this edge, and free to move in the

Table 6 Dimensionless deflection $\overline{w} = 100w_{max}h^3E_{2,Gr-Ep}/(Pa^4)$ of simply supported 6 layer square laminates under unit sinusoidal load

a/h	Lay-Ups	Open-Circuit, Continuous Electrodes	Open-Circuit, Unelectroded	Close-Circuit	Elastic
4	($p/0°/90°/90°/0°/p$)	1.2318	1.2070	1.2708	1.2726
	($p/0°/90°/0°/90°/p$)	1.2208	1.1973	1.2591	1.2608
	($p/45°/-45°/45°/-45°/p$)	1.1749	1.1549	1.2041	1.2057
	($p/45°/-45°/-45°/45°/p$)	1.1813	1.1595	1.2097	1.2114
10	($p/0°/90°/90°/0°/p$)	0.5944	0.5718	0.6277	0.6281
	($p/0°/90°/0°/90°/p$)	0.6013	0.5782	0.6361	0.6366
	($p/45°/-45°/45°/-45°/p$)	0.5303	0.5125	0.5544	0.5547
	($p/45°/-45°/-45°/45°/p$)	0.5292	0.5107	0.5523	0.5526
100	($p/0°/90°/90°/0°/p$)	0.4676	0.4463	0.4995	0.4997
	($p/0°/90°/0°/90°/p$)	0.4816	0.4593	0.5158	0.5161
	($p/45°/-45°/45°/-45°/p$)	0.4053	0.3884	0.4284	0.4286
	($p/45°/-45°/-45°/45°/p$)	0.3999	0.3827	0.4220	0.4222

normal in-plane direction for the (p/0°/90°/0°/90°/p) laminate, or in the tangential in-plane direction for the (p/45°/-45°/45°/-45°/p) laminate, whereas other degrees of freedom are fixed. The electric conditions are identical to the previous example.

The resulting dimensionless deflections $\bar{w} = 100w_{max}h^3E_{2,Gr-Ep}/(Pa^4)$ are given in Table 6. The elastic solutions are also listed for comparison.

It can be noticed that the piezoelectricity has little effects on the deflection of the laminates with closed-circuits, while it reduces w_{max} of the unelectroded laminates with open-circuits by up to 12.4%. The maximum stiffening effect is obtained by the thin (p/0°/90°/0°/90°/p) laminate with a/h=100, even though the (p/45°/-45°/45°/-45°/p) laminate has the best stiffness among the considered fibre orientations.

4. Conclusions

In the present study, the spline finite strip method incorporating different shear deformation theories is successfully developed for the static analysis of piezoelectric composite plates. The analysis was conducted according to Reddy's third-order shear deformation theory, Touratier's "Sine" model, Afaq's exponential model, Cho's higher-order zigzag laminate theory, as well as first order plate theory and classical thin plate theory. The selection of a specific method is done by simply changing a few terms in a 2 by 2 square matrix. Thus, the results based on different plate theories can be compared each other.

The numerical results show that the convergence of the proposed method is satisfactory for piezoelectric composite plates subjected to mechanical loading, and the higher-order shear deformation theories yield significant improved accuracy over the lower-order plate theories at only a little extra computational cost.

In addition, the following findings are revealed from the parametric study:

· The piezoelectricity has little effects on the deflection of the laminate with closed-circuits, while it substantially reduces w_{max} of the simply supported laminate with open-circuits;

· The maximum stiffening effect is achieved for the thin antisymmetric cross-ply laminates, although the antisymmetric angle-ply laminate has the best stiffness among the considered fibre orientations;

· The continuous electrode is inefficient for the clamped laminate, since the piezoelectricity has insignificant stiffening effect in this particular case, and the induced electrode potential is relatively low.

Acknowledgements

References

Afaq, K., Karama, M. and Mistou, S. (2003), "A new refined model for laminated structures", *Comptes Rendus des JNC13*, Strasbourg, France, 12-14 mars, 283-292.

Akhras, G. and Li, W.C. (2005), "Static and free vibration analysis of composite plates using spline finite strips with higher-order shear deformation", *Compos. Part B*, **36**, 496-503.

Akhras, G. and Li, W.C. (2007), "Spline finite strip analysis of composite plates based on higher-order zigzag composite plate theory", *Compos. Struct.*, **78**(1), 112-118.

Akhras, G. and Li, W.C. (2007), "Three dimensional static, vibration and stability analysis of piezoelectric

composite plates using finite layer method", *Smart Mater. Struct.*, **16**(3), 561-569.

Cheung, M.S., Li, W.C. and Chidiac, S.E. (1996), *Finite Strip Analysis of Bridges*, London: E & FN SPON.

Cho, M.H. and Parmerter, R.R. (1993), "Efficient higher order composite plate theory for general lamination configurations", *AIAA J.*, **31**(7), 1299-1306.

Dawe, D.J. (2002), "Use of the finite strip method in predicting the behaviors of composite laminated structures", *Compos. Struct.*, **57**(1), 11-36.

Heyliger, P. (1994), "Static behavior of laminated elastic/piezoelectric plates", *AIAA J.*, **32**, 2481-4.

Kant, T. and Swaminathan, K. (2001), "Analytical solutions for free vibration of laminated composite and sandwich plates based on a higher-order refined theory", *Compos. Struct.*, **53**, 73-85.

Kogl, M. and Bucalem, M.L. (2005), "A family of piezoelectric MITC plate elements", *Compos. Struct.*, **83**(15-16), 1277-1297.

Kong, J. and Cheung, Y.K. (1993), "Application of the spline finite strip to the analysis of shear deformable plates", *Compos. Struct.*, **46**(6), 985-988.

Pagano, N.J. (1970), "Exact solutions for rectangular bidirectional composites and sandwich plates", *J. Compos. Mater.*, **4**(1), 20-34.

Phan, N.D. and Reddy, J.N. (1985), "Analysis of laminated composite plates using a higher-order deformation theory", *Int. J. Numer. Meth. Eng.*, **21**, 2201-2219.

Ramos Loja, M.A., Infante Barbosa, J., Mota Soares, C.M. and Mota Soares, C.A. (2001), "Analysis of piezolaminated plate structures by spline finite strip method", *Compos. Struct.*, **79**, 2321-2333.

Ramos Loja, M.A., Mota Soares, C.M. and Mota Soares, C.A. (2002), "Modelling and design of adaptive structures using B-spline method", *Compos. Struct.*, **57**, 245-251.

Ramos Loja, M.A., Mota Soares, C.M., Mota Soares, C.A. (2001), "Higher-order B-spline finite strip model for laminated adaptive structures", *Compos. Struct.*, **52**, 419-427.

Reddy, J.N. (1984), "A simple higher-order theory for laminated composite plates", *J. Appl. Mech.*, **51**, 745-752.

Reddy, J.N. (2004), *Mechanics of Laminated Composite Plates and Shells: Theory and Analysis*, Second edition, Boca Raton, CRC Press.

Sheikh, A.H. and Chakrabarti, A. (2003), "A new plate bending element based on higher-order shear deformation theory for analysis of composite plates", *Finite Elem. Anal. Des.*, **39**(9), 883-903.

Shu, X.P. and Sun, L.X. (1994), "An improved simple higher-order theory for laminated composite plates", *Compos. Struct.*, **50**(2), 231-236.

Topdar, P., Chakraborti, A. and Sheikl, A.H. (2004), "An efficient hybrid plate model for analysis and control of smart sandwich laminates", *Comput. Method. Appl. M.*, **193**, 4591-4610.

Touratier, M. (1991), "An efficient standard plate-theory", *Int. J. Eng. Sci.*, **29**(8), 901-916.

CC

Appendix. Coefficients in $\overline{Q}$ Matrix (Kogl and Bucalem 2005, Kant and Swaminathan 2001, Reddy 2004)

The material properties of a lamina are usually given in the local 1-2-3 system, in which 1 and 2 respectively denote the fibre and transverse to fibre in-plane directions, while 3 refers to the direction normal to the plate midplane. In three dimensional analysis, the relationships between the generalized stresses and generalized strains in this system are stated as:

$$
\begin{Bmatrix} \sigma_1 \\ \sigma_2 \\ \sigma_3 \\ \tau_{12} \\ \tau_{23} \\ \tau_{31} \\ D_1 \\ D_2 \\ D_3 \end{Bmatrix} = \begin{bmatrix} C_{11} & C_{12} & C_{13} & & & & & & e_{31} \\ C_{12} & C_{22} & C_{23} & & & & & & e_{32} \\ C_{13} & C_{23} & C_{33} & & & & & & e_{33} \\ & & & G_{12} & & & & & \\ & & & & G_{23} & & & e_{24} & \\ & & & & & G_{31} & e_{15} & & \\ & & & & & e_{15} & -\eta_{11} & & \\ & & & & e_{24} & & & -\eta_{22} & \\ e_{31} & e_{32} & e_{33} & & & & & & -\eta_{33} \end{bmatrix} \begin{Bmatrix} \varepsilon_1 \\ \varepsilon_2 \\ \varepsilon_3 \\ \gamma_{12} \\ \gamma_{23} \\ \gamma_{31} \\ -E_1 \\ -E_2 \\ -E_3 \end{Bmatrix}
\tag{A1}
$$

where C_{ij} are calculated from Young's moduli E_i and Poisson's ratios v_{ij} (i, j=1 to 3) as:

$$C_{11} = E_1(1 - v_{23}v_{32})/\Delta, \quad C_{12} = E_1(v_{21} + v_{31}v_{23})/\Delta$$

$$C_{13} = E_1(v_{31} + v_{21}v_{32})/\Delta, \quad C_{22} = E_2(1 - v_{13}v_{31})/\Delta$$

$$C_{23} = E_2(v_{32} + v_{12}v_{31})/\Delta, \quad C_{33} = E_3(1 - v_{12}v_{21})/\Delta$$

and

$$\Delta = 1 - v_{12}v_{21} - v_{23}v_{32} - v_{13}v_{31} - 2v_{12}v_{23}v_{31},$$

$$v_{12}/E_1 = v_{21}/E_2, v_{23}/E_2 = v_{32}/E_3, v_{13}/E_1 = v_{31}/E_3,$$

whereas

$$\eta_{ii} = k_i\eta_0 \text{ for } i = 1, 2, 3$$

with k_i being dielectric constant, and $\eta_o = 8.8541878176 \times 10^{-12}$ F/m denoting the permittivity of free space.

Since σ_3 is neglected in the present analysis, ε_3 in the matrix equation (A1) can be eliminated by assuming $\sigma_3 = 0$. Thus, the first, the second and the last equations in (A1) are reduced to:

$$\sigma_1 = C_{11}^*\varepsilon_1 + C_{12}^*\varepsilon_2 - e_{31}^*E_3$$

$$\sigma_2 = C_{12}^*\varepsilon_1 + C_{22}^*\varepsilon_2 - e_{32}^*E_3$$

$$D_3 = e_{31}^*\varepsilon_1 + e_{32}^*\varepsilon_2 - \eta_{33}^*E_3$$

where

$$C_{11}^* = C_{11} - \frac{(C_{13})^2}{C_{33}}, C_{12}^* = C_{12} - \frac{C_{13}C_{23}}{C_{33}}, C_{22}^* = C_{22} - \frac{(C_{23})^2}{C_{33}},$$

$$e_{31}^* = e_{31} - \frac{C_{13}}{C_{33}}e_{33}, e_{32}^* = e_{32} - \frac{C_{23}}{C_{33}}e_{33}, \eta_{33}^* = \eta_{33} + \frac{(e_{33})^2}{C_{33}}$$

After coordinate transformation, the relationships between the generalized stresses and generalized strains in the global x-y-z system are obtained as expressed by Eq. (17). The items of $\overline{Q}$ matrix are computed as:

$$\overline{Q}_{11} = C_{11}^* c^4 + 2(C_{12}^* + 2G_{12})s^2c^2 + C_{22}^* s^4$$

$$\overline{Q}_{12} = C_{12}^*(c^4 + s^4) + (C_{11}^* + C_{22}^* - 4G_{12})s^2c^2$$

$$\overline{Q}_{16} = (C_{11}^* - C_{12}^* - 2G_{12})sc^3 + (C_{12}^* - C_{22}^* + 2G_{12})cs^3$$

$$\overline{Q}_{22} = C_{11}^* s^4 + 2(C_{12}^* + 2G_{12})s^2c^2 + C_{22}^* c^4$$

$$\overline{Q}_{26} = (C_{11}^* - C_{12}^* - 2G_{12})s^3c + (C_{12}^* - C_{22}^* + 2G_{12})c^3s$$

$$\overline{Q}_{66} = (C_{11}^* - 2C_{12}^* + C_{22}^* - 2G_{12})c^2s^2 + G_{12}(c^4 + s^4)$$

$$\overline{Q}_{44} = G_{23}c^2 + G_{31}s^2$$

$$\overline{Q}_{45} = (G_{31} - G_{23})sc$$

$$\overline{Q}_{55} = G_{31}c^2 + G_{23}s^2$$

$$\bar{e}_{31} = e_{31}^* c^2 + e_{32}^* s^2, \qquad \bar{e}_{32} = e_{31}^* s^2 + e_{32}^* c^2,$$

$$\bar{e}_{33} = e_{33}^*, \qquad \bar{e}_{36} = (e_{31}^* - e_{32}^*)sc$$

$$\bar{e}_{14} = (e_{15} - e_{24})sc, \qquad \bar{e}_{15} = e_{15}c^2 + e_{24}s^2$$

$$\bar{e}_{24} = e_{24}c^2 + e_{15}s^2, \qquad \bar{e}_{25} = (e_{15} - e_{24})sc$$

$$\eta_{xx} = \eta_{11}c^2 + \eta_{22}s^2, \qquad \eta_{yy} = \eta_{11}s^2 + \eta_{22}c^2$$

$$\eta_{xy} = (\eta_{11} - \eta_{22})sc, \qquad \eta_{zz} = \eta_{33}^*$$

where $c = \cos\theta$, $s = \sin\theta$, and θ denotes the angle measured anticlockwise from the x axis to the 1 axis.